Aeolian Research 12 (2014) 9–17

Contents lists available at ScienceDirect

Aeolian Research

journal homepage: www.elsevier.com/locate/aeolia

Detecting surface moisture in aeolian environments using terrestrial laser scanning

Joanna M. Nield [a,*], James King [b], Benjamin Jacobs [c]

[a] University of Southampton, Geography and Environment, Highfield, Southampton SO171BJ, UK
[b] University of Oxford, School of Geography and the Environment, Oxford University Centre for the Environment, South Parks Road, Oxford OX13QY, UK
[c] University of Bonn, Department of Geography, Bonn D-53115, Germany

ARTICLE INFO

Article history:
Received 14 June 2013
Revised 25 October 2013
Accepted 28 October 2013
Available online 17 November 2013

Keywords:
Terrestrial laser scanning (TLS)
Soil moisture
Aeolian transport
Playa salt crust
Beach sand
Distance calibration

ABSTRACT

Surface moisture plays a key role in determining erodibility of sandy and dusty surfaces in semi-arid and coastal environments. Where aeolian processes are active, sedimentation patterns may rapidly change the soil moisture on a thin veneer of the surface that determines sediment entrainment. Here we present terrestrial laser scanning (TLS) as a promising method for detecting moisture at high temporal and spatial resolution within the range where aeolian transport is possible and illustrate its applicability using playa and beach case studies. TLS instruments are active sensors that record the return intensity (or backscatter) of a laser pulse. This signal intensity is influenced by both distance and surface properties. Calibration relationships are outlined that correct for both distance and moisture and explore the influence of grain size and mineralogy. We also show that by normalising intensity using a dry surface, the resulting relative ratio infers changes in moisture patterns and is a useful alternative when sediment calibrations are not available.

1. Introduction

Accurately quantifying surface moisture in semi-arid and coastal environments is vital because moisture is a key controlling factor in aeolian sand and dust transport initiation (Sarre, 1988; Namikas and Sherman, 1995; McKenna Neuman and Scott, 1998; Wiggs et al., 2004; Davidson-Arnott et al., 2005). Surface moisture increases the shear velocity threshold required to entrain sediment and so it is important to be able to accurately account for surface moisture in dust emission modelling (Marticorena and Bergametti, 1995; McTainsh et al., 1998; Fecan et al., 1999) and dune sedimentation balances (Bauer and Davidson-Arnott, 2003; Davidson-Arnott et al., 2008; Bauer et al., 2009; Davidson-Arnott and Bauer, 2009; Hesp et al., 2009; Delgado-Fernandez and Davidson-Arnott, 2009; Walker et al., 2009a,b). While measurement techniques such as soil moisture probes can be very useful at elucidating spatial patterns between the intertidal zone and back beach area (Oblinger and Anthony, 2008; Edwards and Namikas, 2009; Anthony et al., 2009; Namikas et al., 2010; Schmutz and Namikas, 2011) they only measure depth-averaged moisture content. This can be problematic in low moisture environments where it is only the very thin veneer of surface particles which are important for determining sediment transport (Darke et al., 2009; Nield et al., 2011). Instead, non-invasive remote sensing methods that assess the top of the surface can give a more representative measure of surface moisture important for sediment entrainment.

Synoptic remote sensing methods assess surface properties at a range of scales including (i) coarse resolution (hundreds of metres) satellite imagery over large areas (e.g. Scheidt et al., 2010), (ii) pole mounted camera systems at the meso-scale (tens of metres) (e.g. Delgado-Fernandez et al., 2009; Darke et al., 2009; Lorenz et al., 2010; McKenna Neuman and Langston, 2006), and (iii) hand-held spectrometers at the micro-scale (sub metre) (e.g. Edwards et al., 2012, 2013). Whilst these image and spectral based methods are able to provide detailed surface moisture maps, they lack the ability to differentiate changes in topography and so their predictive capabilities for aeolian transport remain poorly constrained for actively migrating individual landforms (Namikas et al., 2010). This is in part due to the high spatial variability of surface moisture and the interactions and feedback between moisture, surface texture and sedimentation patterns in active transport environments. For example, in sandy environments, the development of sand strips and protodunes can result in either increased or decreased transport when gravimetric moisture content is below 810% (Hotta et al., 1984; Jackson and Nordström, 1998; Nield et al., 2011; Nield and Wiggs, 2011; Delgado-Fernandez et al., 2012). In dust source areas such as playas, changes in above surface relative humidity can occur rapidly with a change in temperature overnight (Saint-Amand et al., 1986; Scheidt et al., 2010), and this change in relative

* Corresponding author. Tel.: +44 23 8059 4749.
E-mail address: J.Nield@soton.ac.uk (J.M. Nield).

1875-9637/$ - see front matter © 2013 Elsevier B.V. All rights reserved.
http://dx.doi.org/10.1016/j.aeolia.2013.10.006

humidity can modify surface moisture (Mahowald et al., 2003; Reheis and Urban, 2011) and crust characteristics (Archer and Wadge, 2001; Reynolds et al., 2007). It is therefore imperative to undertake experiments at the meso-scale (20–100 m) that include co-located measurements of surface morphology and moisture, in order to characterise the heterogeneous nature of surfaces and their feedbacks and better link this to large scale observations (Legates et al., 2011).

Terrestrial laser scanning (TLS) is a technique whereby spatial coordinates of a surface can be measured remotely in a short time (minutes) over a moderate area (10 s of square metres), without interfering with the surface being measured (Buckley et al., 2008). In addition to spatial metrics, the signal return intensity (or backscatter) is also recorded (Lichti, 2005). This co-located intensity measurement is a function of surface properties and instrument position and can be calibrated to surface moisture (Kaasalainen et al., 2008; Franceschi et al., 2009; Nield et al., 2011; Gonzalez-Jorge et al., 2012). TLS techniques offer a way to examine feedbacks between surface properties and transport processes in areas where small changes in sedimentation may have a large influence on surface moisture and the resulting sediment entrainment potential. Return signal intensity is also influenced by other environmental attributes such as distance to target (Lichti, 2003, 2005; Kaasalainen et al., 2008, 2011; Wang and Lu, 2009), mineralogy (Franceschi et al., 2009; Armesto-González et al., 2010; Burton et al., 2011; Nield et al., 2013) and grain size (Kaasalainen et al., 2011) and there are few studies that report on the influence of these factors (Franceschi et al., 2009; Kaasalainen et al., 2011; Eitel et al., 2011).

Here we undertake a number of controlled and in situ experiments to investigate the response of TLS return signal intensity to changes in surface moisture of aeolian sediments. First, we compare the distance response of the TLS signal to different grain size and mineralogy and develop generic distance calibration relationships for aeolian sediments. Second, we quantify the relationship between TLS return signal intensity and gravimetric moisture. We calibrate the signal to measured moisture and develop relative and direct intensity ratio methods that can be used as a moisture proxy when field measurements are not available. Third, we illustrate how the methodologies developed in this paper can be used to indicate sediment availability in coastal environments.

2. TLS data collection methodologies

Nine different sediments were examined to investigate TLS return signal intensity response to (i) environmental attributes (distance, grain size and mineralogy) and (ii) surface moisture through in situ and controlled experiments. In situ experiments were undertaken on sand (Set A) and playa (Set B) surfaces and excluded any active transport or elevation change to limit the focus of this study to surface moisture rather than topographic response.

2.1. TLS field sites

Set A experiments investigated the response of sand surface to in situ wetting and drying (Table 1). Surface wetting after a moderate rain storm was examined at Ynyslas beach (A1), on the central western coast of Wales, UK near Aberystwyth (site location: 52.53°N 4.06°W). Measurements were taken in July 2008 on a stretch of beach above the high tide extent, bounded to the south-east by a dune system and to the north-west by a small patch of nebkha dunes that extended towards the intertidal zone (see Nield et al., 2011 for more details of the field location). Increased moisture after light rain was examined using an inland example at Great Sand Dunes (A2), in Colorado, USA (site location: 37.694°N 105.585°W). Measurements were taken in May 2010 on the unvegetated stoss slope of an actively migrating parabolic dune, south of the main dune field (see Lorenz and Valdez (2011) for more details of the site location). Surface response to drying (A3) was examined on an intertidal beach surface at East Head, which is a sandy spit (May and Hansom, 2003) on the south coast of the UK, near Chichester (site location: 50.785°N 0.915°W) in August 2009. Measurements were taken below the high tide mark, west of the coast bordering dunes.

Set B experiments measured surfaces with varying moisture content at the same field site (Table 1). Damp and dry salt crust surfaces were measured at Sua Pan, Botswana (site location: 20.575°S 25.959°E), during August in 2011 and 2012. Sua Pan is a 3400 km^2 wet playa with a predominantly halite crust (Eckardt et al., 2008) and it is situated within the Makgadikgadi Pan which is one of southern Africa's largest dust source areas (Prospero et al., 2002; Washington et al., 2003; Zender and Kwon, 2005). The surfaces examined in this paper were relatively flat and homogenous in surface roughness and included newly formed smooth salt crust (maximum roughness element height <7 mm), and older, degraded surfaces (roughness element mean height 8–12 mm).

2.2. Terrestrial laser scanner

Data collection in the field and controlled experiments was undertaken using a time-of-flight Leica Scanstation, except for field location measurements at A2 where a Leica Scanstation 2 was used. The Scanstation is not sensitive to antecedent illumination. It utilises a green laser (wavelength 532 nm) with a sampling frequency of 4000 points/s, a laser footprint of 4 mm at 50 m and an approximate precision of 2 mm (Hodge et al., 2009). Point cloud data is recorded in the form of x, y and z coordinates and intensity of the return signal. Raw intensity values are stored as 16-bit digital numbers and these were converted to standard intensity values between 0 and 1 following the methods of Franceschi et al. (2009) and Eitel et al. (2011). Mixed pixels can reduce return signal intensity if partial returns are recorded. This effect was reduced by spatial averaging, over 1 cm for the high resolution salt pan field experiment and 10 cm for the lower resolution Ynyslas beach experiment following the methods of Nield et al. (2011, 2013). Appropriate averaging size depends on the scan resolution and the angularity of the surface, as sharp edges may increase the number of mixed pixels. The averaging sizes used in this study were smaller than the scale of the visually observed surface moisture patterns and measured surface microtopography (salt crust average element spacing ranged between 56 and 223 mm and beach sand strips are typically >1 m).

2.3. Controlled experiments

A number of controlled experiments were conducted to examine the relationship between natural sand and salt pan surfaces and distance and grain size effects (Experiments 1a and b, Table 1). Sediment samples were analysed from each of the field locations as well as sediment from inland nebkha dune crests (C1), interdune areas (C2) and a flat, vegetated creosote site (C3). Additional samples of green glass (D1) and sea salt granules (D2) were also examined. Dry sediment was placed on 1 cm deep trays (20 × 30 cm) and measured using the Scanstation at Euclidian distances between 20 and 35 m with a specified point spacing of 2 mm. A section of scanned points 20 cm wide were extracted from the TLS point cloud for each distance increment and average and standard deviation intensity values were determined within each section. Salt crust samples extracted from Sua Pan were measured in a similar way, but the actual salt crust sections were approximately 10 cm wide. Mean point densities within each sample were

Table 1
Overview of the different experiment aims, relevant sediment samples and related figures.

Experiment					Sample										Related figures
Type	Number	Description	Controlled experiment	Insitu	A1	A2		A3	B		C1	C2	C3	D1	D2	
					Beach	Continential dune		Beach	Playa salt crust		Nebkha dune crest	Nebkha interdune	Creosote (non-dune)	Green glass beads	Sea salt granules	
						Wet	Dry		Wet	Dry						
Environmental attributes	1a	Grain size influence on signal intensity	x		x		x	x			x	x	x			1
	1b	Distance calibration of signal intensity	x	x	x	x	x	x	x	x	x	x	x	x	x	2, 3
Moisture	2a	Surface moisture using relative intensity ratio (Method 1)		x	x	x		x	x	x						5, 6, 8, 9
	2b	Surface moisture using direct intensity ratio (Method 2)		x	x				x	x						4, 5, 6, 8, 9
	2c	Surface moisture calibration	x		x									x		7
Application	3	Change in erodibility in response to changes in surface moisture		x	x											10

12 points cm^{-2}. Euclidian distance was calculated between the centre of the sediment sample and the head of the TLS laser.

Controlled experiments were also undertaken to calibrate TLS signal intensity to gravimetric moisture using green glass granules (D1) and beach sand (A1) (Experiment 2 c). Two 1 cm deep trays were filled with sand, positioned alongside each other and scanned at a distance of 20 m from an elevated location. A single scan was completed over approximately 2 min, after which 4 mm surface scrapings were bagged and moisture measured gravimetrically following the method of Wiggs et al. (2004). The control tray remained dry, whilst well-mixed sediment samples with varying moisture content (0–10%) were placed in the second tray. These moist samples were pre-mixed prior to placement in the tray and were immediately scanned and sampled. As in the distance experiment, a section of scanned points 20 cm wide corresponding to the position and size of the sediment surface sampler were extracted from the TLS point cloud for each moisture increment.

2.4. Relative surface moisture using TLS intensity ratios

The use of TLS data normalised by co-located points collected at a different time has shown promise in comparing surface change on rock surfaces and glacial debris coverage (Burton et al., 2011; Nield et al., 2013) and is an alternative to reference target normalisation (e.g. Eitel et al. (2011)). These ratio values exclude any distance effects when considering points from the same location and so a lower ratio indicates increased surface moisture and a higher value indicates decreased surface moisture.

Intensity ratios were calculated in two different ways. In Method 1 (Experiment 2a; Table 1) the expected value of the return signal intensity for a dry surface was calculated based on the dry distance calibration (from the results of the controlled experiment equation – Table 2). This is referred to as the 'relative' ratio approach. The expected value was compared to the measured value because the intensity intercept decreases under increased moisture. In the 'direct' ratio approach (Method 2; Experiment 2b; Table 1), the ratio of the uncorrected intensity values pre and post wetting for co-located points at the same Euclidian distance were calculated to infer the change in surface moisture over time. Method 2 requires a temporal sequence of TLS measurement, while Method 1 can be applied to any surface where a dry distance calibration is known. These ratios were assessed using in situ experiments of natural (Set A) or controlled (Set B) surface wetting. For the controlled field response 1×1 m sections of salt crust were moistened with known volumes of water (Data Set B; 400 and 800 ml).

3. Characterising TLS return signal intensity response (Experiments 1 and 2)

3.1. Grain size analysis

Grain size analysis for each of the aeolian sediments was undertaken using a Saturn II particle size analyser (Fig. 1; Table 2). The beach sands from A1 and A3 were well sorted and had similar modes. Inland dune sands from the C1 and A2 were also well

Table 2
Coefficients for distance relationships of dry sediment samples between 20 and 35 m and grain size data (secondary mode in parentheses).

Sample	Gradient	Intercept	R^2	Grain size mode (μm)
Continental dune (A2)	−0.0026	0.546	0.996	355
Nebkha interdune (C2)	−0.0027	0.546	0.990	316 (668)
Nebkha dune crest (C1)	−0.0027	0.549	0.996	298
Beach (A1)	−0.0029	0.563	0.992	224
Beach (A3)	–	–	–	211
Green glass (D1)	−0.0033	0.572	0.988	300
Creosote (non-dune) (C3)	−0.0031	0.580	0.999	251
Sea salt granules (D2)	−0.0038	0.602	0.988	–
Playa salt crust (B)	−0.0040	0.653	0.997	–

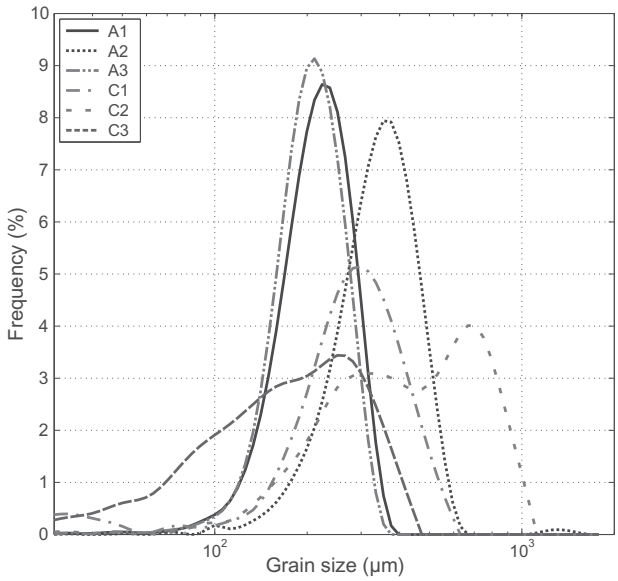

Fig. 1. Grain size distributions for typical wind-blow sand samples (beach: A1 and A3, continental dune: A2, nebkha dune crest: C1, interdune: C2, creosote (non-dune): C3).

sorted but had coarser modes. Sediments from the interdune and vegetated sites (C2 and C3) were not as well sorted and had coarser and finer modes, respectively, compared to the beach samples.

3.2. Distance, mineralogy and grain size influence (Experiment 1)

In aeolian landscapes sediment surfaces are generally rough with respect to laser spot size (Pesci and Teza, 2008; Franceschi et al., 2009), and so the returned light is diffuse (Carrascosa et al., 1985). Therefore the influence of incidence angle is minor and the distance between the object and the instrument is the main control on signal intensity attenuation (Pesci and Teza, 2008; Franceschi et al., 2009; Kaasalainen et al., 2011). For Leica Scanstations, at distances less than 20 m, the intensity increases with distance, whilst for distances greater than 20 m from the sensor return signal intensity decreases with distance (Fig. 2). Uniformly wet or dry playa and sand surfaces show the same overall behaviour in return signal intensity with distance. Individual intensity measurements were averaged over 10 cm intervals to minimise mixed pixel influence. The standard deviations (error bars on Fig. 2) indicate consistent small fluctuations within the 10 cm intervals. The damp salt crust had a reduced intensity value compared to the dry surface due to moisture content which is examined in more detail below.

Similar to observations by other researchers (e.g. Lichti, 2003, 2005; Wang and Lu, 2009; Franceschi et al., 2009), there is a non-linear response of intensity at distances less than 20 m (Fig. 2). However, at distances of between 20 and 35 m, behaviour between measured dry sediment sample intensity and Euclidean distance is strongly linear (e.g. Nield et al., 2011). The effect of grain size and mineralogy over this distance range was investigated in a number of controlled experiments (Fig. 3) to determine the gradient and intercept of each dry material. These relationships are indicated in Table 2. All sand sediments give similar gradients (mean = −0.0028). Salt samples also had similar gradients (mean = −0.0039), but were more reflective than the aeolian quartz sands. Within the sand group, the A1 beach sand in close proximity to a salt source had a higher intensity intercept than the continental sands of A2 and C1. Intensity values are also influenced by grain size (Kaasalainen et al., 2011). Agreement between the intercept values of C1 and C2 suggest that the intensity return signal for well sorted aeolian sand in active transport environments is not influenced by coarser fractions. When finer sediment was available (C3 and A1), grain packing was more efficient because finer grains infill the voids between larger grains, forming a smoother surface. This decrease in small scale surface roughness reduced scatter and increased the intensity of the return signal. Similarly, the intensity intercept value for the salt crust, with a well packed surface, was higher than the sea salt granules.

3.3. Field measurements and estimating the relative change in moisture using intensity ratio (Experiments 2 a and b)

In situ measurements (Set A) all indicated a decrease in intensity ratio with increased moisture (Fig. 4). The A3 inter-tidal exam-

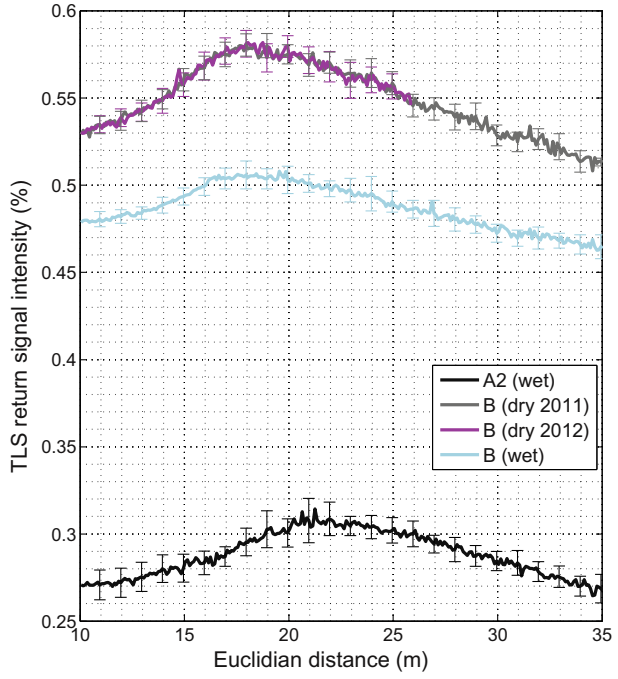

Fig. 2. Variation of signal intensity with Euclidian distance for relatively homogeneous actual field surfaces of wet sand (A2) and different salt pan surfaces (B). Error bars indicate standard deviations.

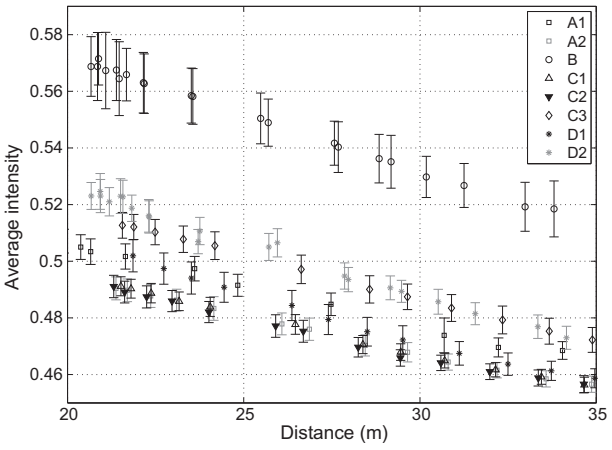

Fig. 3. TLS intensity and distance relationships for different types of dry sand (A1, A2, C1, C2, C3), salt crust samples (B), green glass (D1) and sea salt granules (D2) between 20 and 35 m.

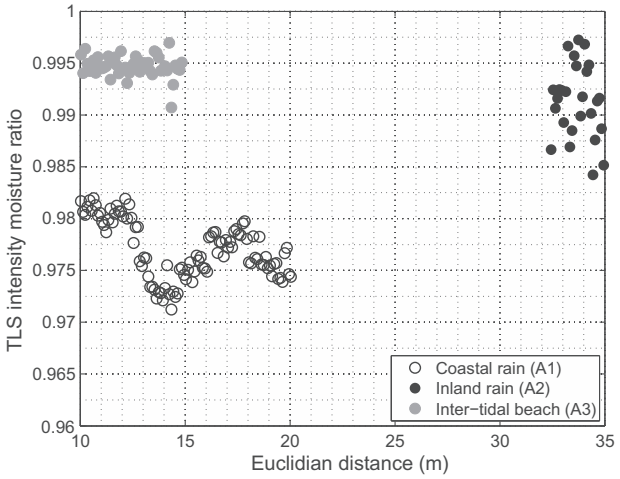

Fig. 4. Intensity ratios (Method 2) used to infer moisture without distance calibration for beach (A1 and A3) and dune (A2) sand with relatively homogeneous wetting due to precipitation or inter-tidal exposure. Rain examples had varying intensity and pre-existing moisture. Inland example was light rain on an already moist dune surface; coastal example was heavy rain on a previously wet surface that had experienced intermittent drying. Inter-tidal beach example was between the berm and mid-tide area and measured over a 2-h time interval. The rain and intertidal measurements are repeated over the same surface from the same location.

ple was most consistent due to the more uniform behaviour of subsurface moisture and atmospheric evaporation rates, in agreement with visual and photographic observations. The coastal (A1) and inland (A2) data sets exhibited more variation due to greater spatial heterogeneity prior to the rain as well as the randomness of rain coverage.

The ratio Method 1 for two different salt crust sections showed a progressive decrease in intensity for sites moistened with 400 and 800 ml of water, respectively (Figs. 5 and 6a–f). Small variations on the control surface were due to topographically controlled moisture patterns that related to ridged (drier) and flat (wetter) areas. The direct ratio approach (Method 2; Figs. 5 and 6g–i) produced maps of relative moisture increase that were strongly correlated to the maps produced using Method 1 (coefficient = 0.94), indicating ratio comparisons are a suitable method to infer relative moisture change when calibration information is unavailable.

3.4. Controlled moisture experiment and using the moisture ratio for field estimations (Experiment 2c)

A strong power relationship exists for each of the two control experiment data sets (A1 (Eq. (1)) and D1 (Eq. (2))) between gravimetric water content and average intensity ($R^2 = 0.92$; Fig. 7). When the results from both these datasets are combined, the power relationship ($R^2 = 0.87$) is given in Eq. (3).

$$W = 4 \times 10^{-19} S^{-63.29} \quad (1)$$

$$W = 8 \times 10^{-30} S^{-103.4} \quad (2)$$

$$W = 1 \times 10^{-21} S^{-72.8} \quad (3)$$

where W is the gravimetric moisture content (%) and S is the TLS return signal intensity (corrected for distance).

The intensity values have small standard deviations and can discriminate within 1–2% gravimetric moisture content over the lower gravimetric moisture content range between 0% and 6% (Fig. 7). This is important as it is the range where other studies suggest the threshold for grain entrainment is likely to occur in many

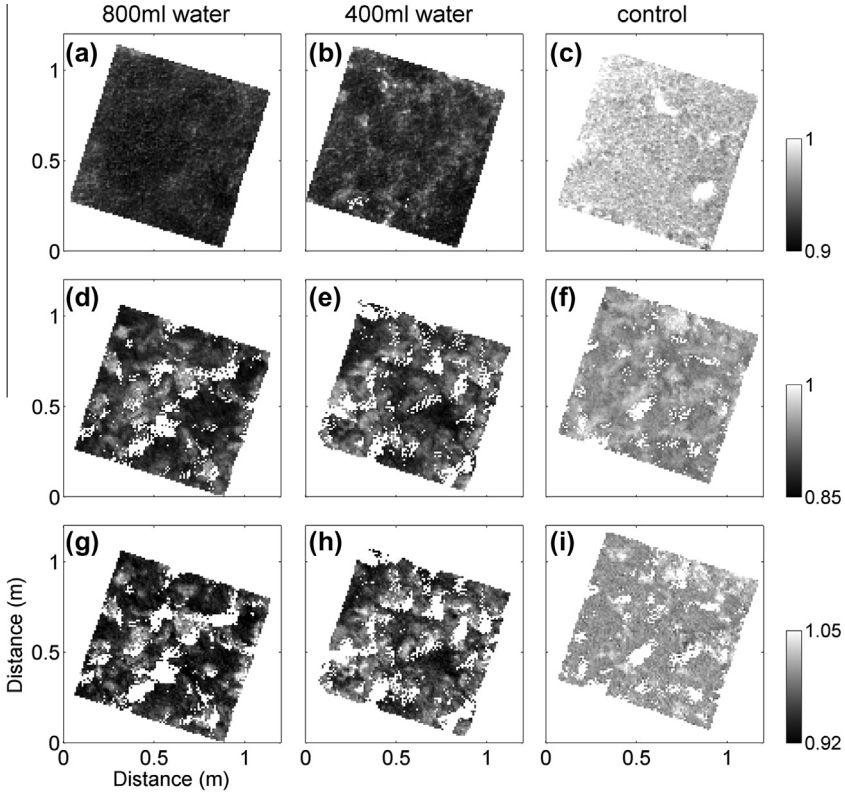

Fig. 5. Salt crust wetting examples (left 800 ml/m^2; centre 400 ml/m^2; right 0 ml/m^2). (a-f) Coloured by 'relative' ratio (Method 1) calculated based on actual measured intensity of wet/control surface and distance corrected intensity value for a dry surface. (g–i) 'direct' ratio (Method 2) of actual measured intensity post and pre water application for the same surfaces shown in d–f. See Fig. 6 for corresponding histograms.

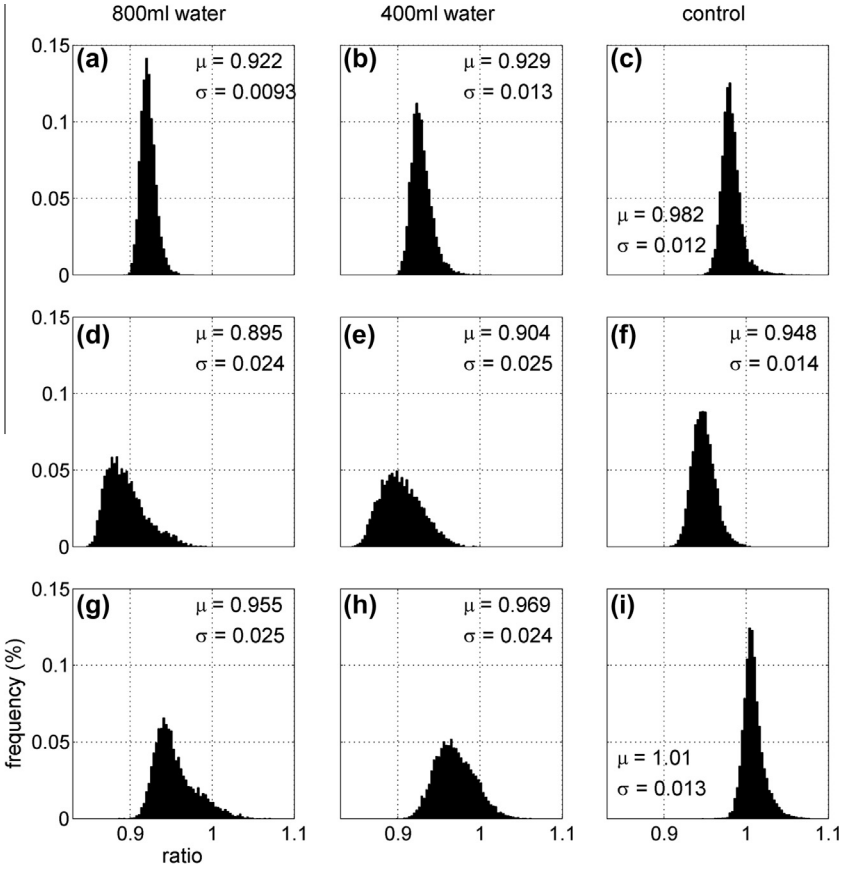

Fig. 6. Histograms of ratios for the salt crust wetting examples (Fig. 5). (a–f) Relative ratio (Method 1) calculated based on actual measured intensity of wet/control surface and distance corrected intensity value for a dry surface. (g–i) Direct ratio (Method 2) of actual measured intensity post and pre water application for the same surfaces shown in Fig. 5d–f. Mean and standard deviation of ratio values indicated by μ and σ, respectively.

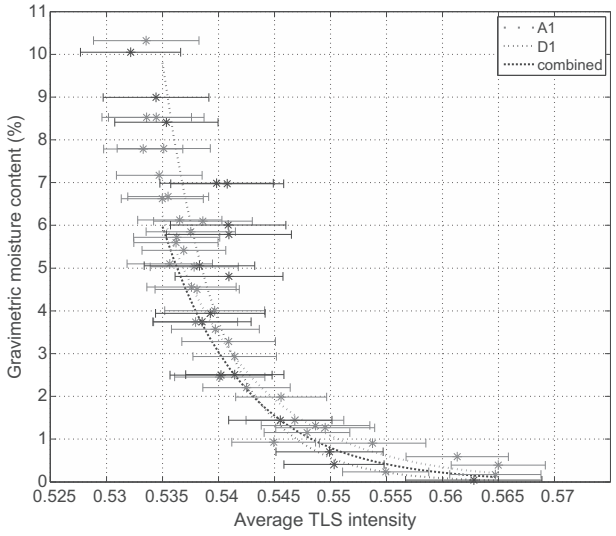

Fig. 7. Variation of signal intensity with gravimetric moisture measurements for two different sediment types (beach sand: A1 and green glass beads: D1). Dashed lines indicate line of best fit for each data set. Error bars indicate standard deviations.

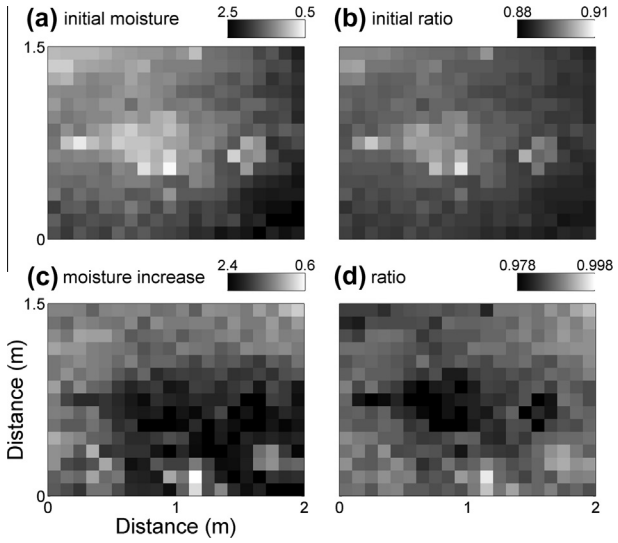

Fig. 8. Initial surface moisture (top; a, b) and change in beach surface moisture (bottom; c, d) after 3 h of rain at A1 inferred by actual gravimetric moisture (left; a, c) calculated from controlled experiments and intensity ratio (right; b (Method 1), d (Method 2)).

environmental situations (Namikas and Sherman, 1995) and transport is seen to be particularly sensitive to changes in moisture content (Wiggs et al., 2004; Bauer et al., 2009).

Surface moisture calculated for the rain event at A1 using ratios (Methods 1 and 2) and control experiment derived moisture indicate similar surface patterns (Fig. 8). The overall increase in moisture, calculated using Eq. (1) and the direct ratio (Method 2) have a correlation of 0.65 and perform best over sections of the surface where the soil was initially dry (Fig. 8 d). On soils with high

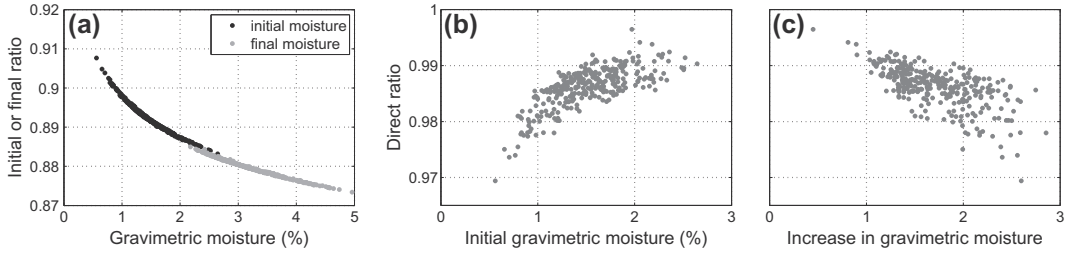

Fig. 9. Relationships between control experiment derived surface moisture before and after a rain event at A1 and the ratio methods. In (a) initial and final moisture are calculated using the relative ratio (Method 1), and in (b) and (c) the direct ratio (Method 2) is compared to surface moisture computed using Eq. (1).

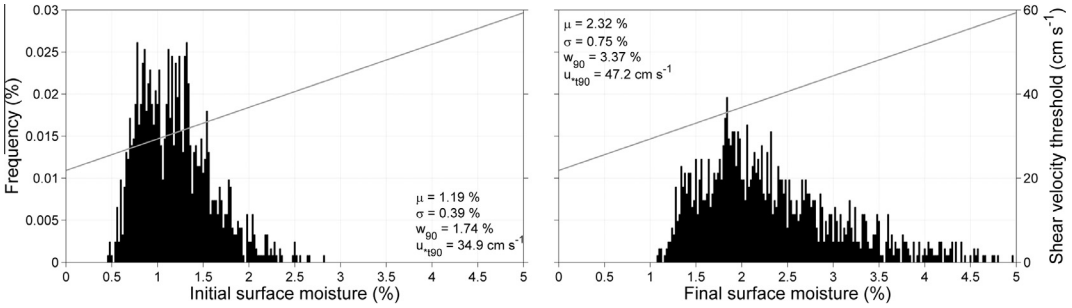

Fig. 10. Surface moisture distributions on a beach section (12.6 m^2) before and after a rain event at A1. Shear velocity threshold for different moisture content indicated by the grey line. Mean and standard deviation of surface moisture values indicated by μ and σ, respectively. Ninetieth percentiles for the shear velocity threshold and surface moisture indicated by u_{*t90} and w_{90}, respectively.

initial moisture content there is more uncertainty and scatter in the relationships when comparing the relative ratio values (Method 1) of surface moisture before and after the rain event (Fig. 9).

3.5. TLS method limitations and future directions

Although TLS is advantageous over synoptic methods that are unable to gather co-located elevation information, and can better account for surface moisture than probe-based instruments, its high cost may limit widespread usage. Alternative, cheaper, slower systems (Eitel et al., 2013) have been developed to monitor vegetation in situ over long time periods (months) and these could provide new insights for coastal or playa surface temporal and spatial patterns when installed in conjunction with camera equipment. TLS measurements are currently limited to small areas (e.g. tens of metres) to enable sampling times below the spatial scale of surface change, but as technology advances, TLS sampling rates continue to increase and larger areas can be measured at a speed exceeding rates of surface change. New TLS instruments with moisture sensitive (e.g. infra-red) or multispectral wavelengths in the future may also improve our ability to detect surface moisture change over a greater range of values and with higher precision.

4. Estimating surface erodibility (Experiment 3)

Spatial information from TLS measurements can be used to assess the erodibility of a surface based on the surface moisture modification to shear velocity thresholds. This then enables the determination of relationships between surface sedimentation and moisture change. Wind conditions were calm at the A1 study site during the field experiment, so here we illustrate the change in shear velocity threshold over the beach due to rain only. The shear velocity threshold for dry sand was calculated using the Bagnold (1941) Eq. (4). This was then converted to a threshold for different surface moisture contents using the Hotta et al. (1984) relationship Eq. (5).

$$u_{*ct} = A\sqrt{\frac{(\rho_s - \rho_a)gd}{\rho_a}} \tag{4}$$

$$u_{*ctw(Hotta)} = u_{*ct} + 7.5W \tag{5}$$

where u_{*ct} and u_{*ctw} are the critical shear velocities for dry and wet sand respectively, ρ_s and ρ_a are the sediment and air densities respectively, d is grain diameter, g is acceleration due to gravity, and A is a constant, assumed to be 0.1 at fluid threshold.

Fig. 10 highlights the usefulness of TLS data calibrated by using the controlled experiment to determine surface moisture response to rain. During the initial scan, 90% of a 12.6 m^2 beach surface had a moisture content below 1.74%, so the minimum shear velocity required to mobilise 90% of the surface was 34.9 cm s^{-1}. After the heavy rain shower, this 90% shear velocity threshold increased to 47.2 cm s^{-1}. The surface moisture distribution after rain was also wider, indicating greater variability in moisture cover (standard deviations increased from 0.39% to 0.75%).

5. Conclusions

TLS is a useful tool for measuring spatial and temporal change in surface moisture, particularly in aeolian environments where these changes may be fast and intrinsically linked. When the surface is initially dry, relative change sufficiently indicates areas with increased moisture irrespective of the actual intensity measurement. If dry surface measurements are not available, then the ratio inferred from controlled experiment distance corrected intensity is a suitable alternative to establish surface moisture patterns in sandy or crusted soils. The application of TLS in aeolian environments has the potential to elucidate erosivity and erodibility feedback relationships as surface topography and moisture patterns co-evolve.

Acknowledgements

Thanks to many field and laboratory assistants including C.S. Bristow, S.E. Darby, F.D. Eckardt, C.R. Hackney, N. Lancaster, J. Leyland, P. Morgan, R. Pomeroy, L. Riddy, R.S. Squirrell, A. Valdez, J.M. Wheaton, G.F.S. Wiggs, RT Wilson and logistics funding that assisted in making field sample collection possible (Royal Society (TG092278), British Society for Geomorphology (BSG: Wiley-Blackwell ESPL Fund), World University Network Mobility Grant, University of Southampton FSHS Strategic Research Development Fund, NERC DO4Models (NE/H021841/1)). Thanks for permission to use field sites at Ynyslas, East Head and Great Sand Dunes National Park and Preserve to M. Bailey and Countryside Council for Wales, A. Lawrence and the National Trust and F. Bunch, A. Valdez and the US National Park Service. Some of the data processing was undertaken using the IRIDIS High Performance Computing Facility at the University of Southampton. Helpful comments from I. Delgado-Fernandez and two anonymous reviewers are greatly appreciated.

References

Anthony, E.J., Ruz, M.H., Vanhee, S., 2009. Aeolian sand transport over complex intertidal bar-trough beach topography. Geomorphology 105, 95–105.
Archer, D.J., Wadge, G., 2001. Modeling the backscatter response due to salt crust development. IEEE Transactions on Geoscience and Remote Sensing 39, 2307–2310.
Armesto-González, J., Riveiro-Rodríguez, B., González-Aguilera, D., Rivas-Brea, M.T., 2010. Terrestrial laser scanning intensity data applied to damage detection for historical buildings. Journal of Archaeological Science 37, 3037–3047.
Bagnold, R.A., 1941. The Physics of Blown Sand and Desert Dunes. Chapman and Hall, London, p. 265.
Bauer, B.O., Davidson-Arnott, R.G.D., 2003. A general framework for modeling sediment supply to coastal dunes including wind angle, beach geometry, and fetch effects. Geomorphology 49, 89–108.
Bauer, B.O., Davidson-Arnott, R.G.D., Hesp, P.A., Namikas, S.L., Ollerhead, J., Walker, I.J., 2009. Aeolian sediment transport on a beach: surface moisture, wind fetch, and mean transport. Geomorphology 105, 106–116.
Buckley, S.J., Howell, J.A., Enge, H.D., Kurz, T.H., 2008. Terrestrial laser scanning in geology: data acquisition, processing and accuracy considerations. Journal of the Geological Society 165, 625–638.
Burton, D., Dunlap, D.B., Wood, L.J., Flaig, P.P., 2011. Lidar intensity as a remote sensor of rock properties. Journal of Sedimentary Research 81, 339–347.
Carrascosa, M., Cusso, F., Agullo-Lopez, F., 1985. Lambert emitters: a simple Monte Carlo approach to optical diffusers. European Journal of Physics 6, 186–187.
Darke, I., Davidson-Arnott, R., Ollerhead, J., 2009. Measurement of beach surface moisture using surface brightness. Journal of Coastal Research 25, 248–256.
Davidson-Arnott, R.G.D., Bauer, B.O., 2009. Aeolian sediment transport on a beach: thresholds, intermittency, and high frequency variability. Geomorphology 105, 117–126.
Davidson-Arnott, R.G.D., MacQuarrie, K., Aagaard, T., 2005. The effect of wind gusts, moisture content and fetch length on sand transport on a beach. Geomorphology 68, 115–129.
Davidson-Arnott, R.G.D., Yang, Y., Ollerhead, J., Hesp, P.A., Walker, I.J., 2008. The effects of surface moisture on aeolian sediment transport threshold and mass flux on a beach. Earth Surface Processes and Landforms 33, 55–74.
Delgado-Fernandez, I., Davidson-Arnott, R., 2009. Sediment input to foredunes: description and frequency of transport events at Greenwich Dunes, PEI, Canada. Journal of Coastal Research SI 56, 302–306.
Delgado-Fernandez, I., Davidson-Arnottt, R., Ollerhead, J., 2009. Application of a remote sensing technique to the study of coastal dunes. Journal of Coastal Research 25, 1160–1167.
Delgado-Fernandez, I., Davidson-Arnott, R., Bauer, B.O., Walker, I.J., Ollerhead, J., Rhew, H., 2012. Assessing aeolian beach-surface dynamics using a remote sensing approach. Earth Surface Processes and Landforms n/a.
Eckardt, F.D., Bryant, R.G., McCulloch, G., Spiro, B., Wood, W.W., 2008. The hydrochemistry of a semi-arid pan basin case study: Sua Pan, Makgadikgadi, Botswana. Applied Geochemistry 23, 1563–1580.
Edwards, B.L., Namikas, S.L., 2009. Small-scale variability in surface moisture on a fine-grained beach: implications for modeling aeolian transport. Earth Surface Processes and Landforms 34, 1333–1338.
Edwards, B.L., Schmutz, P.P., Namikas, S.L., 2012. Comparison of surface moisture measurements with depth-integrated moisture measurements on a fine-grained beach. Journal of Coastal Research, in press.
Edwards, B.L., Namikas, S.L., D'Sa, E.J., 2013. Simple infrared techniques for measuring beach surface moisture. Earth Surface Processes and Landforms 38, 192–197.
Eitel, J.U.H., Vierling, L.A., Long, D.S., Hunt, E.R., 2011. Early season remote sensing of wheat nitrogen status using a green scanning laser. Agricultural and Forest Meteorology 151, 1338–1345.
Eitel, J.U.H., Vierling, L.A., Magney, T.S., 2013. A lightweight, low cost autonomously operating terrestrial laser scanner for quantifying and monitoring ecosystem structural dynamics. Agricultural and Forest Meteorology 180, 86–96.
Fecan, F., Marticorena, B., Bergametti, G., 1999. Parametrization of the increase of the aeolian erosion threshold wind friction velocity due to soil moisture for arid and semi-arid areas. Annales Geophysicae-Atmospheres Hydrospheres and Space Sciences 17, 149–157.
Franceschi, M., Teza, G., Preto, N., Pesci, A., Galgaro, A., Girardi, S., 2009. Discrimination between marls and limestones using intensity data from terrestrial laser scanner. ISPRS Journal of Photogrammetry and Remote Sensing 64, 522–528.
Gonzalez-Jorge, H., Gonzalez-Aguilera, D., Rodriguez-Gonzalvez, P., Arias, P., 2012. Monitoring biological crusts in civil engineering structures using intensity data from terrestrial laser scanners. Construction and Building Materials 31, 119–128.
Hesp, P.A., Walker, I.J., Namikas, S.L., Davidson-Arnott, R., Bauer, B.O., Ollerhead, J., 2009. Storm wind flow over a foredune, Prince Edward Island, Canada. Journal of Coastal Research 1, 312–316.
Hodge, R., Brasington, J., Richards, K., 2009. In situ characterization of grain-scale fluvial morphology using Terrestrial Laser Scanning. Earth Surface Processes and Landforms 34, 954–968.
Hotta, S., Kubota, S., Katori, S., Horikawa, K., 1984. Sand Transport by Wind on a Wet Sand Surface. American Society of Civil Engineers, New York, pp. 1265–1281.
Jackson, N.L., Nordström, K.F., 1998. Aeolian transport of sediment on a beach during and after rainfall, Wildwood, NJ, USA. Geomorphology 22, 151–157.
Kaasalainen, S., Kukko, A., Lindroos, T., Litkey, P., Kaartinen, H., Hyyppa, J., Ahokas, E., 2008. Brightness measurements and calibration with airborne and terrestrial laser scanners. Geoscience and Remote Sensing, IEEE Transactions on 46, 528–534.
Kaasalainen, S., Jaakkola, A., Kaasalainen, M., Krooks, A., Kukko, A., 2011. Analysis of incidence angle and distance effects on terrestrial laser scanning intensity: search for correction methods. Remote Sensing 3, 2207–2221.
Legates, D.R., Mahmood, R., Levia, D.F., DeLiberty, T.L., Quiring, S.M., Houser, C., Nelson, F.E., 2011. Soil moisture: a central and unifying theme in physical geography. Progress in Physical Geography 35, 65–86.
Lichti DD. 2003. Modelling of laser scanner NIR intensity for multi-spectral point cloud classification. pp. 282–290.
Lichti, D., 2005. Spectral filtering and classification of terrestrial laser scanner point clouds. The Photogrammetric Record 20, 218–240.
Lorenz, R.D., Valdez, A., 2011. Variable wind ripple migration at Great Sand Dunes National Park and Preserve, observed by timelapse imaging. Geomorphology 133, 1–10.
Lorenz, R.D., Jackson, B., Barnes, J.W., 2010. Inexpensive time-lapse digital cameras for studying transient meteorological phenomena: dust devils and playa flooding. Journal of Atmospheric and Oceanic Technology 27, 246–256.
Mahowald, N.M., Bryant, R.G., del Corral, J., Steinberger, L., 2003. Ephemeral lakes and desert dust sources. Geophysical Research Letters 30.
Marticorena, B., Bergametti, G., 1995. Modeling the atmospheric dust cycle: 1. Design of a soil-derived dust emission scheme. Journal of Geophysical Research: Planets 100, 16415–16430.
May, V.J., Hansom, J.D., 2003. Coastal geomorphology of Great Britain. Joint Nature Conservation Committee, 63, p. 737.
McKenna Neuman, C., Langston, G., 2006. Measurement of water content as a control of particle entrainment by wind. Earth Surface Processes and Landforms 31, 303–317.
McKenna Neuman, C., Scott, M.M., 1998. A wind tunnel study of the influence of pore water on aeolian sediment transport. Journal of Arid Environments 39, 403–419.
McTainsh, G.H., Lynch, A.W., Tews, E.K., 1998. Climatic controls upon dust storm occurrence in eastern Australia. Journal of Arid Environments 39, 457–466.
A review of the effects of surface moisture content on aeolian sand transport, 1995. In: Tchakerian, V.P. (Ed.). Desert Aeolian Processes. Chapman and Hall, New York, pp. 269–293.
Namikas, S.L., Edwards, B.L., Bitton, M.C.A., Booth, J.L., Zhu, Y., 2010. Temporal and spatial variabilities in the surface moisture content of a fine-grained beach. Geomorphology 114, 303–310.
Nield, J.M., Wiggs, G.F.S., 2011. The application of terrestrial laser scanning to aeolian saltation cloud measurement and its response to changing surface moisture. Earth Surface Processes and Landforms 36, 273–278.
Nield, J.M., Wiggs, G.F.S., Squirrell, R.S., 2011. Aeolian sand strip mobility and protodune development on a drying beach: examining surface moisture and surface roughness patterns measured by terrestrial laser scanning. Earth Surface Processes and Landforms 36, 513–522.
Nield, J.M., Chiverrell, R.C., Darby, S.E., Leyland, J., Vircavs, L.H., Jacobs, B., 2013. Complex spatial feedbacks of tephra redistribution, ice melt and surface roughness modulate ablation on tephra covered glaciers. Earth Surface Processes and Landforms 38, 94–102.
Oblinger, A., Anthony, E.J., 2008. Surface moisture variations on a multi-barred macrotidal beach: implications for aeolian sand transport. Journal of Coastal Research 24, 1194–1199.
Pesci, A., Teza, G., 2008. Effects of surface irregularities on intensity data from laser scanning: an experimental approach. Annals of Geophysics 51, 839–848.

Prospero, J.M., Ginoux, P., Torres, O., Nicholson, S.E., Gill, T.E., 2002. Environmental characterization of global sources of atmospheric soil dust identified with the Nimbus 7 Total Ozone Mapping Spectrometer (TOMS) absorbing aerosol product. Reviews of Geophysics 40, 2-1–2-31.

Reheis, M.C., Urban, F.E., 2011. Regional and climatic controls on seasonal dust deposition in the southwestern US. Aeolian Research 3, 3–21.

Reynolds, R.L., Yount, J.C., Reheis, M., et al., 2007. Dust emission from wet and dry playas in the Mojave desert, USA. Earth Surface Processes and Landforms 32, 1811–1827.

Saint-Amand, P., Mathews, L.A., Gaines, C., Reinking, R., 1986. Dust Storms from Owens and Mono Valleys. Naval Weapons Center, California.

Sarre, R.D., 1988. Evaluation of aeolian sand transport equations using intertidal zone measurements, Saunton Sands, England. Sedimentology 35, 671.

Scheidt, S., Ramsey, M., Lancaster, N., 2010. Determining soil moisture and sediment availability at White Sands Dune Field, New Mexico, from apparent thermal inertia data. Journal of Geophysical Research: Planets 115, F02019.

Schmutz, P.P., Namikas, S.L., 2011. Utility of the Delta-T theta probe for obtaining surface moisture measurements from beaches. Journal of Coastal Research, 478–484.

Walker, I.J., Davidson-Arnott, R.G.D., Hesp, P.A., Bauer, B.O., Ollerhead, J., 2009a. Mean flow and turbulence responses in airflow over foredunes: new insights from recent research. Journal of Coastal Research 1, 366–370.

Walker, I.J., Hesp, P.A., Davidson-Arnott, R.G.D., Bauer, B.O., Namikas, S.L., Ollerhead, J., 2009b. Responses of three-dimensional flow to variations in the angle of incident wind and profile form of dunes: Greenwich Dunes, Prince Edward Island, Canada. Geomorphology 105, 127–138.

Wang, C.K., Lu, Y.Y., 2009. Potential of ILRIS3D intensity data for planar surfaces segmentation. Sensors 9, 5770–5782.

Washington, R., Todd, M., Middleton, N.J., Goudie, A.S., 2003. Dust-storm source areas determined by the total ozone monitoring spectrometer and surface observations. Annals of the Association of American Geographers 93, 297–313.

Wiggs, G.F.S., Baird, A.J., Atherton, R.J., 2004. The dynamic effects of moisture on the entrainment and transport of sand by wind. Geomorphology 59, 13–30.

Zender, C.S., Kwon, E.Y., 2005. Regional contrasts in dust emission responses to climate. Journal of Geophysical Research-Atmospheres 110, D13201.